Journal of Applied Electrochemistry **30**: 1033–1041, 2000.

Photocatalytic degradation of oxalic acid on a semiconductive layer of *n*-TiO_2 particles in a batch plate reactor. Part III: Rate determining steps and nonsteady diffusion model for oxygen transport

J. KRÝSA[1], K. BOUZEK[1] and Ch. STOLLBERG[2]
[1]*Institute of Chemical Technology, Department of Inorganic Technology, Technická 5, 166 28 Prague 6, Czech Republic*
[2]*Fachgebiet Elektrotechnologien und Umwelttechnik, Fachhochschule Anhalt, Abteilung Köthen, Bernburger Strasse 52-57, 06366 Köthen, Germany*

Received 23 February 1999; accepted in revised form 27 March 2000

Key words: *n*-TiO_2, oxalic acid, photocatalytic degradation, rate determining steps

Abstract

The effect of oxygen concentration on the photocatalytic degradation rate of oxalic acid on a fixed layer of TiO_2 particles in a batch mode plate photoreactor was investigated at various light intensities. The regions where the photocatalytical decomposition rate is controlled by the flux of oxygen, photons, or both, were identified. For low oxygen concentration (0–0.15 mol m^{-3}) and photon flux intensity in the range from 10 to 24×10^{-5} einstein m^{-2} s^{-1} the experimentally determined photocatalytical decomposition rate was in agreement with that theoretically calculated assuming the process to be controlled by the limiting flux of oxygen to the TiO_2 surface. At higher concentrations of oxygen (0.15–0.94 mol m^{-3}) the rate of photocatalysis was controlled simultaneously by both the flux of oxygen and photons. The influence of the oxygen concentration decreased with decreasing photon flux. For low photon flux intensities ($\leqslant 3.5 \times 10^{-5}$ einstein m^{-2} s^{-1}), the reaction rate was controlled by the photon flux. The concentration profile of oxygen in the diffusion layer along the reactor plate was calculated and showed a significant decrease in oxygen concentration on the TiO_2 surface.

List of symbols

A	active surface of the reactor plate (m^2)
c	concentration (mol m^{-3})
d_f	thickness of the liquid film (m)
D	diffusion coefficient (m^2 s^{-1})
d	distance between reactor plate and sunbed tubes (m)
g	gravity constant (m s^{-2})
h	Planck constant (J s)
J	flux density (mol m^{-2} s^{-1}) or (einstein m^{-2} s^{-1})
k	rate constant of the reaction of oxygen with electron (mol^{1-n} m^{3n-2} s^{-1}), Equation 15
L	length of the reactor plate (m)
n	kinetic order of the reaction of oxygen with electron (1), Equation 15
Q	flow rate (m^3 s^{-1})
$v_y(x)$	linear flow velocity in y direction (m s^{-1})
V_r	total volume of the solution (m^3)
w	width of the reactor plate (m)

Greek symbols

α	inclination angle of the reactor plate to the horizontal (°)
δ	thickness (m)
λ	wavelength of the light (m)
ν	kinematic viscosity (m^2 s^{-1}) or stoichiometric coefficient (l)
τ	time (s)

Subscripts

$(COOH)_2$	oxalic acid
$h\nu$	photons
lim	limiting
N	Nernst
O_2	oxygen
org	organic compound

Superscripts

0	bulk
s	surface

1. Introduction

Semiconductors can act as sensitizers for light-induced redox processes due to their electronic structure [1] which is characterised by the presence of a filled valence band and an empty conduction band. When the photon energy matches, or exceeds, the band gap energy of the semiconductor, an electron is promoted from the

valence band into the conduction band leaving a positive hole behind. Excited-state electrons and valence-band holes can recombine and dissipate the input energy as heat, get trapped in metastable surface states or react with electron donors and electron acceptors adsorbed on the semiconductor particle. The valence-band holes are powerful oxidants (+1.0 to +3.5 V vs SHE depending on the semiconductor and pH) while the conduction-band electrons are good reductants (+0.5 to −1.5 V vs SHE) [2].

Several simple metal oxide and sulfide semiconductors (TiO_2, WO_3, $SrTiO_3$, α-Fe_2O_3, ZnO and ZnS) have bandgap energies sufficiently large for promoting or catalysing a wide range of chemical reactions of environmental interest. However, among these semiconductors titanium dioxide in the anatase form appears to be the most practical [3, 4] for widespread environmental applications such as water purification, wastewater treatment, hazardous waste control, air purification and water disinfection. TiO_2 is biologically and chemically inert, stable with respect to photocorrosion and chemical corrosion and inexpensive. The main disadvantage is, however, a too high band gap energy (about 3.2 eV), which reduces the solar light harvesting efficiency down to about 5%. In recent years, Degussa P25 TiO_2 has set the standard for photoreactivity in environmental applications. It is a nonporous 70%:30% anatase-to-rutile mixture with a BET surface area of 55 ± 12 m^2 g^{-1} and crystalline sizes of 30 nm in 0.1 μm diameter aggregates.

The application of illuminated semiconductors for the removal of contaminants has been used successfully for a wide variety of compounds [5–11] such as alkanes, aliphatic alcohols, carboxylic acids, alkenes, phenols, aromatic carboxylic acids, dyes, PCBs, simple aromatics, halogenated alkanes and alkenes, surfactants, and pesticides. A detailed list of photocatalytically treated contaminants was given by Hoffmann et al. [12]. In many cases, complete mineralisation to simple inorganic products (e.g., CO_2, H_2O, mineral acids) has been reported.

Concerning practical photocatalysis systems the major issues are whether to use suspended or supported photocatalyst, solar or artificial u.v. light and, in the case of solar energy utilisation, whether to use concentrated or nonconcentrated sunlight.

Slurry and supported TiO_2 photocatalysts have been compared using trichloroethylene as a model pollutant [13], the slurry system was found to outperform the supported photocatalyst almost by a factor of two. Since the slurry consists of very fine particles, it requires a very long settlement time for the catalyst to be removed from the purified water, and filtration, centrifugation or coagulation must be employed. These added steps and various levels of complexity to an overall treatment process clearly decrease the economical viability of the slurry reactors.

Consequently, attention has recently turned to the application of immobilised catalysts [14–16], usually in the form of TiO_2 powder attached to the sides of a vessel, which constitutes a flow-through fixed bed reactor [17]. Recently Butterfield et al. [18] used a falling film reactor consisting of a stainless steel pipe coated on the inside surface with TiO_2 sol–gel film.

Christensen and Walker [19] published a review on solar water detoxification processes. The advantages and drawbacks of related techniques were compared and evaluated. As a main conclusion the inability of purely photochemical systems employing TiO_2 photocatalyst to compete with other techniques in the treatment of high-volume water was highlighted. The main drawbacks were low light efficiency (electron-hole recombination), photocatalyst instability under real conditions and high space demands. However, the necessity to perform more systematic engineering study of photo- and photoelectrochemical detoxification systems was emphasized, mainly in connection with complementary multidiscipline techniques.

As oxygen reacts with the trapped electrons, the electron-hole recombination can be suppressed by the enhanced transport of oxygen to the TiO_2 surface. Therefore this has to be considered as one of the rate determining steps. Using TiO_2 slurry this factor can be neglected [20], mainly because of the high interfacial area typical for this configuration. In the case of a fixed TiO_2 layer we have to deal with a different situation since the interfacial area is dramatically reduced. Thus, the study of the influence of oxygen concentration on the photocatalytical decomposition of the model compound may provide important insight into factors influencing the process efficiency. This will allow quantification of the effect of oxygen concentration on the photocatalysis rate.

This work is a continuation of previous studies [21, 22] devoted to the mass transfer limits and photon flux limits in the photocatalytic degradation of oxalic acid. The aim of this work is an experimental determination of regions where the rate of photocatalytic decomposition of organics is controlled by the flux of either oxygen or photons, or by both these factors together. The conclusion, on the basis of experimental results, will be verified by a model for nonsteady diffusion of oxygen in a layer of liquid freely falling on an inclined plate with an immobilised TiO_2 layer. Furthermore, the concentration field of oxygen along the TiO_2 photocatalyst surface will be calculated for different bulk oxygen concentrations.

2. Experimental details

The photoreactor (Figure 1) was constructed from rectangular polymethylmethacrylate trays with troughs at both ends. The trays were dimensioned to accommodate a glass plate 0.6 m long and 0.3 m wide. The whole assembly was supported by a rig with adjustable feet to allow adjustment of the apparatus by an angle of ten degrees towards the horizontal. Above the glass plate, a

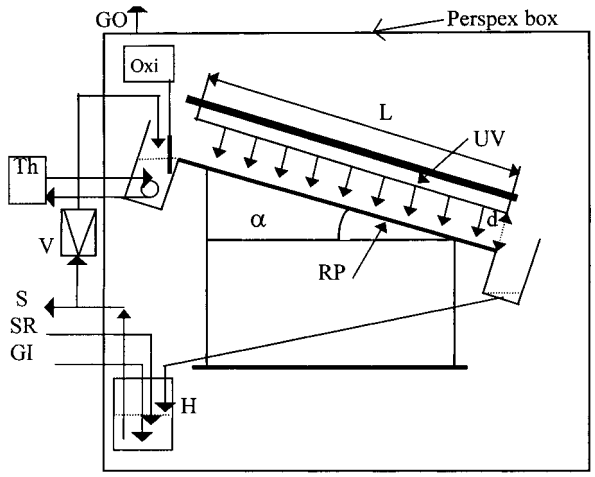

Fig. 1. Schematic representation of the batch mode plate reactor with flow of the solution. Description: (H) holding tank, (V) Venturi tube, UV = 1, 3 or 7 pcs of sunbed tubes, $d = 0.125$ m, (RP) reactor plate of width 0.3 m and length 0.6 m, (α) inclination angle 10°, (GI) gas input, (GO) gas overflow, (S) sampling, (SR) sample return, (Th) thermostat, (Oxi) oxymeter.

parallel plate with one, three or seven ultraviolet sun bed tubes (Osram Eversun L40W/79K, $\lambda = (320 - 385) \times 10^{-9}$ m) was placed. The tubes were adjusted parallel to the length of the plate, 0.125 m above it, and symmetrically from the centre with 0.05 m distances (for seven tubes).

The photon flux on the glass plate of the photoreactor was determined using chemical actinometry. Using the potassium ferrioxalate actinometer [23] a mean photon flux of 3.5×10^{-5} einstein m^{-2} s^{-1} (one tube), 10.2×10^{-5} einstein m^{-2} s^{-1} (three tubes) and 24.4×10^{-5} einstein m^{-2} s^{-1} (seven tubes) was obtained applying the quantum yield 1.21.

Preparation of the TiO_2 layer was similar to that proposed by Bockelmann [17]. The glass plate was degreased and treated in 20% HNO_3 for several days. Then a slightly acidified aqueous suspension of titanium dioxide (P25, Degussa, concentration 10 g dm^{-3}, pH 3) was poured on to the plate. The liquid phase was removed after 3–4 h of sedimentation. The TiO_2 layer was kept at room temperature to dry for the next three days. Finally, it was baked with a stepwise increasing temperature up to 300 °C ± 10 °C for 3 h, after which a slow cooling for 12 h followed. To achieve higher layer thickness the sedimentation and drying was repeated and the layer of required thickness was obtained.

The solution of oxalic acid (initial concentration 5 mol m^{-3}) was pumped from the four litre holding tank (see Figure 1) employing a centrifugal pump (Nova, Sicce, Italy) to the higher trough. The overflow produced a liquid film flowing over the glass plate fixed in the trays. The solution was collected in the lower trough and returned into the holding tank. The flow rate was controlled by a valve and measured using a Venturi tube connected to a mercury filled manometer.

The photoreactor was placed in a closed box with controlled atmosphere. This enabled different oxygen concentrations in the reaction solution of oxalic acid to be attained. The oxygen concentration was followed using an oxymeter Oxi 330 with an oxygen electrode CellOx 325.

For determination of the photocatalysis kinetics, samples of the reaction mixture were taken at various irradiation times and titrated with potassium permanganate. Using this analytical method, oxalic acid remaining in the solution, together with all possible decomposition intermediate products (e.g., HCOOH, HCOH), were determined. For this reason, a direct photocatalytic mineralisation of oxalic acid into carbon dioxide was postulated and the volumes of the $KMnO_4$ solution required were recalculated into equivalent concentrations of oxalic acid.

3. Results

3.1. *Effect of number of TiO_2 layers*

Initially the degradation of oxalic acid was performed on glass plates with various 'thickness' of the immobilised TiO_2 photocatalyst (one, three and five layers). It was found that the degradation flux density was almost the same (i.e., 3.9×10^{-6} mol m^{-2} s^{-1}) in the case of one and three layers for a constant light intensity (seven sun bed tubes) and a constant flow rate (5.5×10^{-5} m^3 s^{-1}) but it increased by about 10% in the case of five TiO_2 layers. The reason is in the increase of layer roughness and subsequently in the increase in mass transfer coefficient and/or absorption of a higher amount of light.

It was reported [14–16] that the use of a fixed TiO_2 film leads to a decreased efficiency of photocatalytic degradation. Where the film is too thick most of the holes are generated too deep in the bulk of the semiconductor to reach the interface. In the case of too thin film only a small part of the incident light will be absorbed. The present results show that the TiO_2 films used in this study were probably between these limits and the observed effect of the layer thickness is small.

3.2. *Effect of oxygen concentration*

The dependence of the oxalic acid concentration on the irradiation time for different bulk concentrations of oxygen and for photon flux intensity 24.4×10^{-5} einstein m^{-2} s^{-1} is shown in Figure 2. The oxalic acid concentration decreases linearly with irradiation time for all the oxygen concentrations. As discussed in [21] this indicates a process not controlled by the transport of oxalic acid to the photocatalyst surface. It is apparent that the absolute value of the slope of the concentration dependence increases with increasing bulk oxygen concentration. This clearly shows that the bulk oxygen concentration strongly effects the degradation rate. The degradation rate was almost negligible at the small

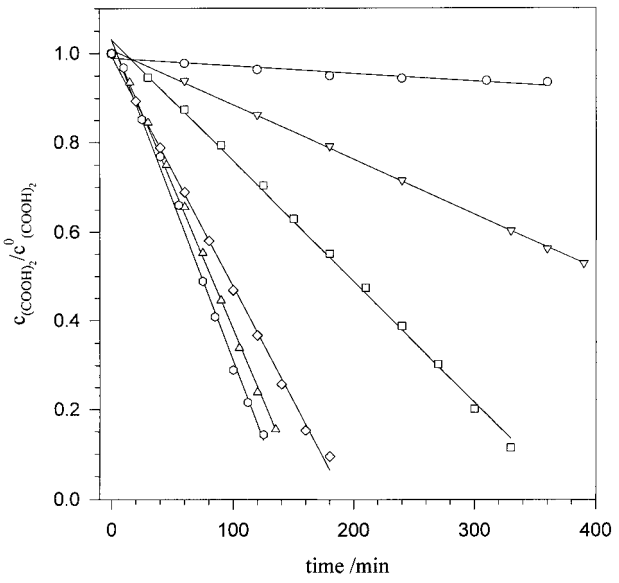

Fig. 2. Dependence of oxalic acid concentration on irradiation time for different bulk concentrations of oxygen. Initial concentration of oxalic acid 5 mol m^{-3}, flow rate 5.5×10^{-5} m^3 s^{-1}, three sun bed tubes (24.4×10^{-5} einstein m^{-2} s^{-1}), $V_r = 0.005$ m^3. $c^o_{O_2}$: (○) 0.0039, (▽) 0.0885, (□) 0.244, (◇) 0.577, (△) 0.773 and (○) 1.143 mol m^{-3}.

oxygen concentration of 0.0039 mol m^{-3} corresponding to a N_2 atmosphere. On the other hand, about two orders higher degradation rate was observed in the case of an oxygen concentration of 1.143 mol m^{-3} which corresponds to a pure O_2 atmosphere.

The dependence of the degradation flux density of oxalic acid on the bulk concentration of oxygen for three different photon flux intensities is shown in Figure 3. The degradation flux density of oxalic acid in a batch mode reactor was calculated from the observed concentration decay using Equation 1:

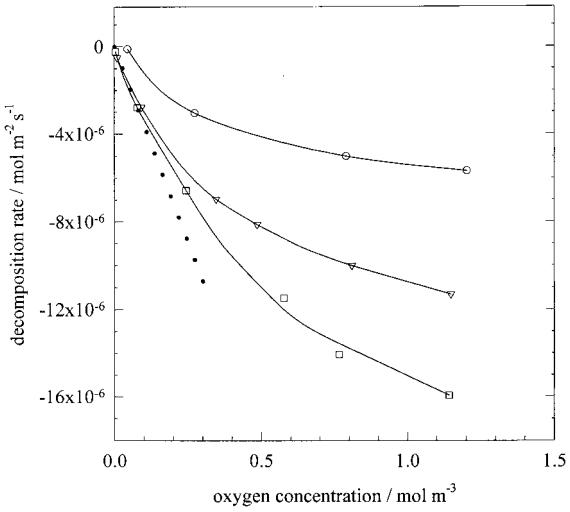

Fig. 3. Dependence of experimental and theoretical flux density of oxalic acid decomposition on bulk concentration of oxygen for three different photon fluxes. Initial concentration of oxalic acid 5 mol m^{-3}, flow rate 5.5×10^{-5} m^3 s^{-1}, $V_r = 0.005$ m^3. Photon flux density: (○) 3.5×10^{-5}, (▽) 10.2×10^{-5} and (□) 24.4×10^{-5} einstein m^{-2} s^{-1}. (••••) Theoretical line limiting O_2 diff. flux.

$$-|J_{org}| = \frac{V_r}{A}\frac{dc_{org}}{d\tau} \quad (1)$$

The validity of Equation 1 was discussed in detail previously [21].

Photocatalytic degradation of oxalic acid on titanium dioxide is a complex physico-chemical process. It starts with absorption of photons by semiconductor particles as a consequence of which pairs of charge carriers – positive holes in the valence band (h^+_{VB}) and electrons in the conduction band (e^-_{CB}) – are formed. The charges can either recombine in the interior of TiO_2 particles or be transferred onto adsorbed molecules or be trapped on the surface, electrons typically on titanium forming Ti(III) species and holes on oxygen producing surface hydroxyl radical groups. These trapped charges can react with reactants diffusing from the aqueous phase and thus redox processes are induced.

In air saturated solutions of oxalic acid, the electron is mainly scavenged by molecular oxygen with formation of superoxide radical anions ($^{\bullet}O_2^-$) while the hole oxidizes oxalic acid to its radical which undergoes a fast Kolbe decarboxylation leading to carbon dioxide as a final product and formyl radical ($^{\bullet}$COOH) as a short lived transient. Unstable radical species can react bimolecularly in two typical ways, recombination and disproportionation, to form stable products and intermediates (e.g., H_2O_2, O_2, HOOC–COOH, HCOOH, CO_2). In the second step, the intermediates can undergo further photocatalytic decomposition on illuminated TiO_2 particles. Hydrogen peroxide can be both oxidised by positive holes back to superoxide radical anion, or reduced by electrons to produce hydroxyl radicals which further contribute to oxidation of the organic molecules present. Although the former oxidation process lowers the photodegradation rate, the latter reduction reaction accelerates it. Formic acid can be oxidized by positive holes with formation of formyl radicals ($^{\bullet}$COOH) which bimolecularly either recombine to oxalic acid or disproportionate to carbon dioxide and formic acid.

Using the mechanism of photocatalytical degradation of oxalic acid postulated in part I and II [21, 22] and the present analysis an overall reaction (2) can be written:

$$2(COOH)_2 + O_2 + \Psi h\nu \rightarrow 4\,CO_2 + 2\,H_2O \quad (2)$$

The total mineralization of two molecules of oxalic acid to four molecules of carbon dioxide and two molecules of water requires one molecule of oxygen. While these stoichiometric proportions are constant, the number of photons per mineralized molecule of oxalic acid ($\Psi/2$) varies according to the reaction conditions. This quantity is dominantly determined by the photophysical events of recombination and trapping of photogenerated charges in semiconductor particles, for example, crystalline structure, particle size, doping, excess of one of the charges, light intensity, pH etc. Photochemical charge transfer plays a minor role in the determination of total quantum yield. Nevertheless, it is important to

investigate rate limiting kinetic factors (e.g., flow rate, photon flux, concentration of oxygen and concentration of organic substances) which influence this quantity and allow optimization of the rate of photocatalytic mineralization.

The flux density of oxygen to the TiO_2 surface can be calculated using Fick's law:

$$J_{O_2} = -D_{O_2} \frac{(c^0_{O_2} - c^s_{O_2})}{\delta_{N,O_2}} \tag{3}$$

where D_{O_2} is the diffusion coefficient of oxygen, $c^0_{O_2}$ the oxygen bulk concentration, $c^s_{O_2}$ the oxygen concentration at the TiO_2 surface and δ_{N,O_2} is the Nernst diffusion layer thickness. For given hydrodynamic conditions (i.e., solution flow rate and viscosity, plate width and inclination), the value of δ_{N,O_2} depends only on the position along the reactor plate and can be calculated according to the following equation [21]:

$$\delta_{N,O_2}(y) = 1.644 \left(\frac{1}{D^3_{O_2} y^3} \frac{Q}{w} \left(\frac{g \sin \alpha}{\nu} \right)^2 \right)^{-1/9} \tag{4}$$

The dependence of thickness δ_{N,O_2} (y) on distance y along the reactor plate is shown in Figure 4 for several ratios of flow rate to plate width (Q/w). It is clear that δ_{N,O_2} (y) decreases with increasing flow rate and decreasing plate width. The factor Q/w was used to emphasize the fact that for constant diffusion coefficient, viscosity and inclination angle the diffusion layer thickness depends only on the volumetric flow rate and plate width.

The average diffusion layer thickness is then given by the equation

$$\delta_{N,O_2} = \frac{1}{L} \int_0^L \delta_{N,O_2}(y) \mathrm{d}y = 1.095 \left(\frac{1}{D^3_{O_2} L^3} \frac{Q}{w} \left(\frac{g \sin \alpha}{\nu} \right)^2 \right)^{-1/9} \tag{5}$$

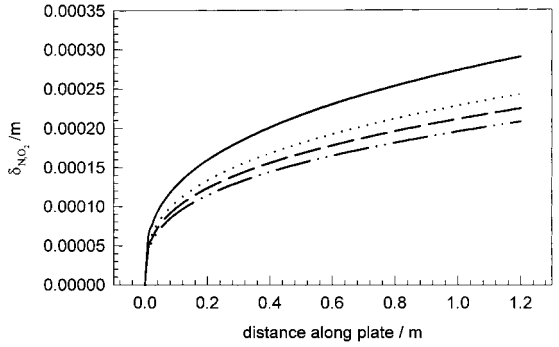

Fig. 4. Thickness of the local Nernst diffusion layer (Equation 4) along the length L for $D_{O_2} = 2.34 \times 10^{-9}$ m^2 s^{-1}, $\nu = 1.0 \times 10^{-6}$ m^2 s^{-1}, $g = 9.81$ m^2 s^{-1}, $\alpha = 10^\circ$ and different ratios of Q/w corresponding to $w = 0.3$ m and $Q = 15$, 75, 150 and 300×10^{-6} m^3 s^{-1}. $(Q/w) \times 10^6$: (——) 50, (· · ·) 250, (– –) 500 and (–·–) 1000 m^2 s^{-1}.

For the case where the rate of oxalic acid degradation is controlled by the flux of oxygen to the TiO_2 surface, the value of $c^s_{O_2}$ approaches zero and the limiting flux of oxygen to the TiO_2 surface is proportional to its bulk concentration. Considering the stoichiometry of Equation 2, the theoretical degradation rate of $(COOH)_2$ can be determined by Equation 6:

$$J_{(COOH)_2,th} = 2 J_{O_2,lim} = -2 D_{O_2} \frac{c^0_{O_2}}{\delta_{N,O_2}} \tag{6}$$

Values of $D_{O_2} = 2.34 \times 10^{-9}$ m^2 s^{-1}, $\nu = 1.0 \times 10^{-6}$ m^2 s^{-1}, $Q = 5.5 \times 10^{-5}$ m^3 s^{-1}, $w = 0.3$ m and $\alpha = 10^0$ were used for calculation of the diffusion layer thickness, δ_{N,O_2}. Applying Equation 6 the oxalic acid decomposition rate corresponding to the limiting flux of oxygen was calculated and is plotted as a broken line in Figure 3.

For low oxygen concentrations (lower than 0.15 mol m^{-3}) and photon flux intensities in the range from 10 to 24×10^{-5} einstein m^{-2} s^{-1}, the experimentally determined rate of photocatalytic decomposition of oxalic acid was in agreement with that theoretically calculated assuming that the process was predominantly controlled by the flux of oxygen to the TiO_2 surface. This confirms our previous theory of rate limiting steps that the rate of photocatalysis is controlled by the oxygen flux under certain conditions.

At higher oxygen concentrations (0.15–0.94 mol m^{-3}), the photocatalysis rate was controlled simultaneously by the both flux of oxygen and photons. The influence of the oxygen concentration decreased with decreasing photon flux. In the case of low photon flux intensities (less than 3.5×10^{-5} einstein m^{-2} s^{-1}), the effect of oxygen concentration on the photocatalysis rate was rather small and the kinetics of the process became controlled mainly by the photon flux.

3.3. *Mathematical model*

The nonsteady diffusion of oxygen in a layer of free falling liquid film is described by Fick's second law:

$$\frac{\partial c_{O_2}}{\partial \tau} = D_{O_2} \frac{\partial^2 c_{O_2}}{\partial x^2} \tag{7}$$

A schematic sketch of the model system with the coordinate system is shown in Figure 5. The value of the liquid flow rate is defined by Equation 8:

$$v_y(x) = \frac{\mathrm{d}y}{\mathrm{d}\tau} \tag{8}$$

Since we consider a laminar flow in the y direction, the linear flow rate in the y direction is a function of the coordinate x and is notated as $v_y(x)$.

Introducing (8) into (7) and rearranging gives:

$$v_y(x) \frac{\partial c_{O_2}}{\partial y} = D_{O_2} \frac{\partial^2 c_{O_2}}{\partial x^2} \tag{9}$$

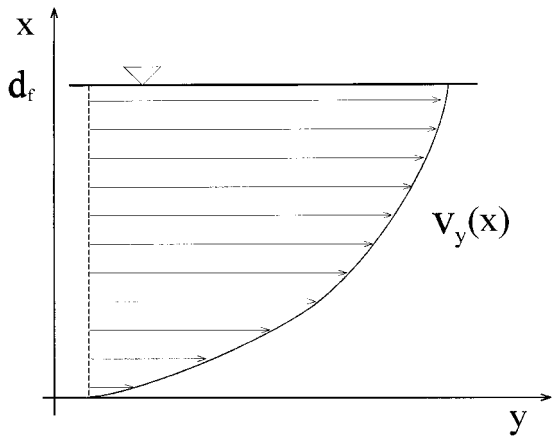

Fig. 5. Schematic sketch of the model system.

This equation can be solved by the method of finite differences using the Crank–Nicholson method:

$$\frac{c_{i,j+1}-c_{i,j}}{\Delta y}=\frac{D_{O_2}}{2v_y(x)}\left(\frac{c_{i+1,j+1}-2c_{i,j+1}+c_{i-1,j+1}}{\Delta x^2}+\frac{c_{i+1,j}-2c_{i,j}+c_{i-1,j}}{\Delta x^2}\right) \quad (10)$$

The subscript index i in Equation 10 and following equations represents a node position along the x axis (along the diffusion layer), whereas the index j represents a node position along the y axis (along the plate). After a simple rearrangement we obtain:

$$-P_i c_{i-1,j+1}+(1+2P_i)c_{i,j+1}-P_i c_{i+1,j+1}=P_i\left[c_{i+1,j}+\left(\frac{1}{P_i}-2\right)c_{i,j}+c_{i-1,j}\right] \quad (11)$$

where

$$P_i=\frac{D_{O_2}}{2v_y(x_i)}\frac{\Delta y}{\Delta x^2} \quad (12)$$

The linear flowrate profile in a laminar film is described by Equation 13:

$$v_y(x_i)=6\bar{v}_y\frac{x_i}{2d_f}\left(1-\frac{x_i}{2d_f}\right) \quad (13)$$

Since Equation 9 is a partial differential equation of second order with respect to x and of the first order with respect to y, the boundary conditions at both ends of the x axis interval and at one end of the studied y axis region must be set. We consider bulk concentration of oxygen to exist at a distance of two local Nernst diffusion layer thicknesses at the end of the plate, Equation 14. The oxygen flux to the TiO_2 surface ($x = 0$) is taken to be equal to its consumption by the reaction with nth order kinetics, Equation 15. At the beginning of the plate, we consider a uniform oxygen concentration across the liquid film, Equation 16.

$$c=c^0_{O_2}\quad y\in\langle 0,L\rangle,\ \ x=2\delta_{N,O2(L)} \quad (14)$$

$$D_{O_2}\frac{\partial c_{O_2}}{\partial x}=k_{O_2}(c^s_{O_2}(y))^n\quad y\in\langle 0,L\rangle,\ \ x=0 \quad (15)$$

$$c=c^0_{O_2}\quad y=0,\ \ x\in\langle 0,2\delta_{N,O2(L)}\rangle \quad (16)$$

where k_{O_2} is a rate constant for the reaction of oxygen with electrons at the TiO_2 surface and $c^s_{O_2}(y)$ is the oxygen concentration at the TiO_2 surface at different positions along the reactor plate. Equation 15 contains a nonlinearity represented by the power n on the oxygen concentration. A Taylor expansion was used to linearise the problem, Equation 17.

$$c^n=c^n_k+nc^{n-1}_k(c_{k+1}-c_k) \quad (17)$$

The subscript k indicates the cycle of iteration of the c^n value. Applying a non-symmetrical finite difference formula and Equation 17, Equation 15 may be converted into the Equation 18:

$$-\left(3+\frac{2nk_{O_2}\Delta x}{D_{O_2}}c^{n-1}_{1,j+1,k}\right)c_{1,j+1,k+1}+4c_{2,j+1}-c_{3,j+1}=\frac{2k_{O_2}\Delta x}{D_{O_2}}c^n_{1,j+1,k}(1-n) \quad (18)$$

The oxygen concentrations at node points across the diffusion layer (i.e., in the x direction with varying i and a constant index j) were calculated using a set of linear equations consisting of Equations 11, 14 and 18. This procedure was repeated for subsequent positions along the y axis, thus providing concentration profiles both across the liquid film and along the reactor.

For the calculation of the concentration profiles, the rate constant k_{O_2} and the reaction order n had to be known. The value of k_{O_2} was iteratively calculated on the basis of the experimentally determined oxalic acid flux (Equation 1) considering the stoichiometry of Equation 2 for different values of n using Equation 19:

$$\frac{1}{L}\int_0^L k_{O_2}(c^s_{O_2}(y))^n dy=J_{O_2}=\frac{1}{2}J_{(COOH)_2} \quad (19)$$

where J_{O_2} is the oxygen consumption flux density and $J_{(COOH)_2}$ is the experimental degradation flux density of oxalic acid.

The calculation of the oxygen profiles was performed for kinetic orders n in the range from 0.05 to 2. Rate constants k_{O_2} calculated for different bulk concentrations of oxygen and for various photon flux densities are shown in Table 1. It can be seen that these values vary, not only with the photon flux, but also with the bulk oxygen concentration. For $n \leqslant 0.125$ the rate constant increases with oxygen concentration. For $a \geqslant 0.5$ the trend is opposite (rate constant for reaction orders 1.5 and 2 are not shown in Table 1 for space reasons). This means that the reason for the change in rate constant is in the incorrectly selected reaction order n. The dividing

Table 1. Calculated values of k_{O_2} for various bulk concentrations of oxygen
Q = 5.5×10^{-5} m^3 s^{-1}, w = 0.3 m, L = 0.6 m

Photon flux density/ einstein m^{-2} s^{-1}	Oxygen bulk concentration /mol m^{-3}	Oxygen flux density $\times 10^6$ /mol m^{-2} s^{-1} (Equation 20)	Reaction rate constants, k_{O_2} as a function of kinetic order $n \times 10^6$ /mol^{1-n} m^{3n-2} s^{-1}				
			$n = 0.05$	$n = 0.125$	$n = 0.25$	$n = 0.5$	$n = 1.0$
3.5×10^{-5}	0.045	0.054949	X	X	X	X	X
	0.273	1.5267	1.655	1.873	2.304	3.486	7.830
	0.791	2.5106	2.558	2.640	2.783	3.092	3.818
	1.203	2.8444	2.831	2.820	2.803	2.768	2.700
10.2×10^{-5}	0.00938	0.2534	X	X	X	X	X
	0.09197	1.388	1.758	2.424	4.117	11.180	94.54
	0.346	3.4808	3.812	4.384	5.533	8.813	22.39
	0.477	4.0641	4.341	4.808	5.701	8.018	15.88
	0.810	5.0091	5.154	5.398	5.830	6.803	9.271
	1.149	5.6603	5.696	5.768	5.891	6.147	6.695
24.4×10^{-5}	0.00391	0.11626	X	X	X	X	5565.0
	0.0781	1.3987	X	X	X	71.34	472.7
	0.0885	1.3713	1.790	2.490	4.323	12.97	112.3
	0.244	3.2832	3.780	4.670	6.621	13.26	52.90
	0.577	5.7302	6.113	6.759	7.988	11.16	21.80
	0.760	6.4078	6.684	7.144	7.982	9.969	15.57
	0.773	7.1465	7.481	8.040	9.065	11.53	18.65
	1.143	7.973	8.092	8.301	8.663	9.437	11.21

line between the two regions is (for the reaction order 0.25) where the rate constants are independent of bulk oxygen concentration. This trend holds for all three photon flux densities. This indicates, that 0.25 is close to the real reaction order. Since values of reaction order were not optimized, 0.25 represents only an approximate value.

For photon flux densities 3.5, 10.2 and 24.4×10^{-5} einstein m^{-2} s^{-1} and oxygen concentrations 0.045, 0.0092 and 0.0039 mol m^{-3}, respectively, the rate constants could not be estimated by the mathematical model. This also applies for photon flux density 24.4×10^{-5} einstein m^{-2} s^{-1} and oxygen concentration 0.0781 mol m^{-3}. This is because in this region the reaction rate is controlled by oxygen transfer to the photocatalyst surface and not by its reaction with electrons. The surface O_2 concentration decreases to zero and the boundary condition, Equation 15 is no more valid (for mass transfer controlled process the correct boundary condition is $c^s_{O_2}(y) = 0$).

A nonintegral reaction order indicates a heterogeneous reaction in the porous structure decelerated by internal diffusion. It shows that oxygen must diffuse into the TiO_2 layer to scavenge electrons [24].

A calculated oxygen concentration profile across the diffusion layer along the reactor plate for a photon flux density of 24.4×10^{-5} einstein m^{-2} s^{-1} and for a bulk concentration of oxygen of 0.24 mol m^{-3} is shown in Figure 6. For this calculation, n was taken as 0.25. It can be seen that the surface oxygen concentration decreases rapidly along the reactor length, for example, in 4 cm decreases from 0.24 to 0.10 mol m^{-3} and then gradually decreases down to 0.05 mol m^{-3} at the end of the reactor. The average surface concentration was about 1/3 of the bulk concentration. This confirms that at high photon flux densities and/or low bulk oxygen concentrations the decrease in surface concentration to a value close to zero factually occurs and the photocatalytic degradation rate is controlled by the oxygen flux.

The oxygen concentration at the TiO_2 surface for different positions along the reactor plate and for variable bulk concentrations is shown in Figures 7, 8 and 9 for various photon flux densities, namely 3.5, 10.2 and 24.4×10^{-5} einstein m^{-2} s^{-1}, respectively, and reaction order 0.25. To obtain the oxygen concentration at the TiO_2 surface, a line parallel to the horizontal axis

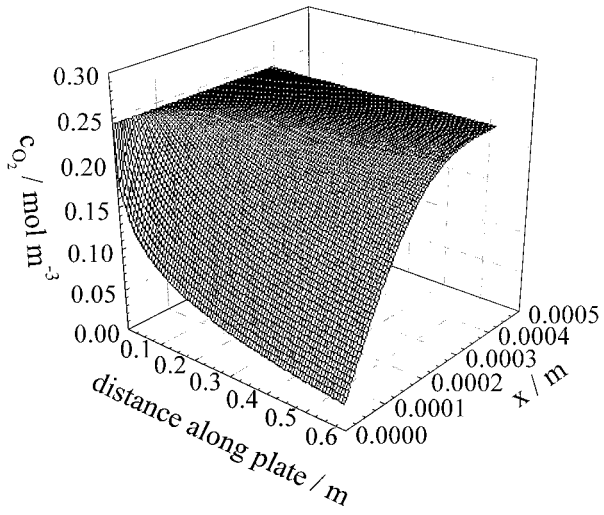

Fig. 6. Concentration profile of oxygen near the TiO_2 surface along the reactor for a bulk concentration of oxygen 0.24 mol m^{-3} and a photon flux intensity of 24.4×10^{-5} einstein m^{-2} s^{-1}. Other conditions see caption to Figure 3.

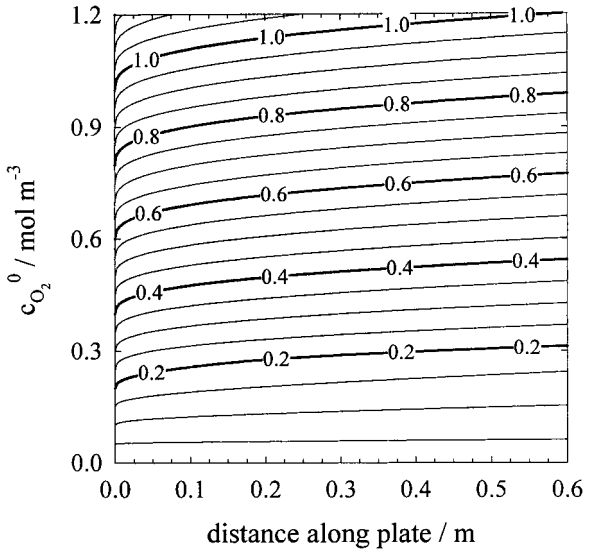

Fig. 7. Dependence of surface concentration of oxygen on position along the reactor plate for a photon flux intensity 3.5×10^{-5} einstein m^{-2} s^{-1} and different bulk concentrations of oxygen. Other conditions see caption to Figure 3.

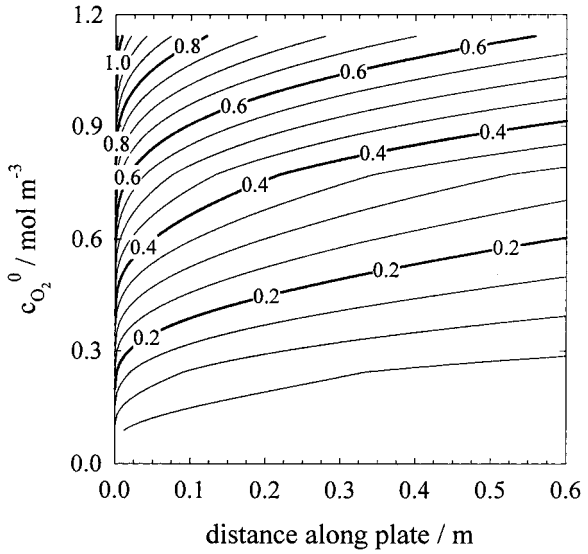

Fig. 9. Dependence of surface concentration of oxygen on position along the reactor plate for a photon flux intensity 24.4×10^{-5} einstein m^{-2} s^{-1} and different bulk concentrations of oxygen. Other conditions see caption to Figure 3.

starting at the vertical axis at a particular value of the oxygen bulk concentration has to be drawn (this value is also on the surface at the beginning of the reactor plate, that is, for $y = 0$). The intersections of this line with the isocurves then show the surface oxygen concentration for different positions along the reaction plate, that is, for varying y.

The surface concentration of oxygen along the reactor plate varies with light intensity. For the lowest photon flux density 3.5×10^{-5} einstein m^{-2} s^{-1} the surface concentration decreases slowly and at the end of the plate reaches 0.18 mol m^{-3} (for bulk concentration 0.3 mol m^{-3}) and 0.72 mol m^{-3} (for bulk concentration 0.9 mol m^{-3}). For the highest photon flux density 24.4×10^{-5} einstein m^{-2} s^{-1} the decrease in surface concentration along the plate is much faster. It is clear that with increasing photon flux density the difference between bulk and surface oxygen concentration increases.

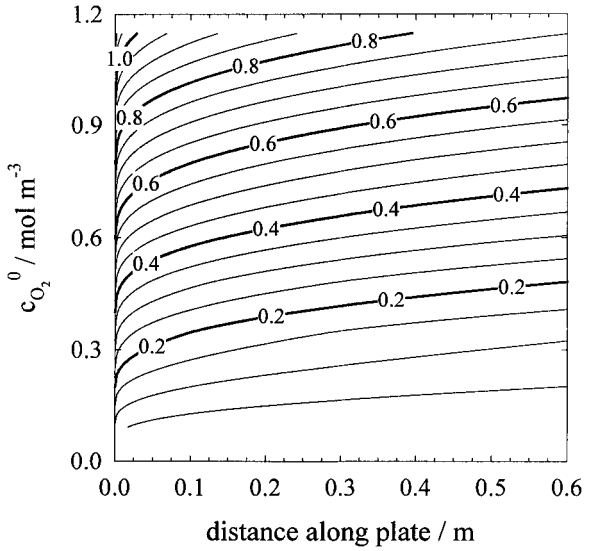

Fig. 8. Dependence of surface concentration of oxygen on position along the reactor plate for a photon flux intensity 10.2×10^{-5} einstein m^{-2} s^{-1} and different bulk concentrations of oxygen. Other conditions see caption to Figure 3.

3.4. *Implications for reactor design*

There are several parameters which effect the degradation rate in the proposed solar reactor: light intensity, oxygen concentration, flow rate, inclination and reactor length.

(i) Increase in TiO_2 thickness has no effect on the degradation rate. This means that a relatively thin TiO_2 layer is sufficient for u.v. light absorption and induction of photocatalytic reaction.

(ii) Inclination of the plate is important. Increase in inclination leads to an increase in degradation rate. The optimal range is 10–20°.

(iii) The positive effect of oxygen bubbling on the efficiency of photocatalytic degradation was experimentally confirmed. Due to oxygen depletion in the liquid film near the TiO_2 surface bubbling of air into the treated solution (bubbling of oxygen would be prohibitively expensive) is necessary to keep the oxygen concentration near the equilibrium value.

(iv) Increase in flow rate results in a decrease of the diffusion layer thickness for oxygen diffusion and an increase in the degradation rate.

4. Conclusion

The regions where the reaction rate is controlled either by the flux of oxygen or by the flux of photons or by

both these factors together have been identified. For oxygen concentrations less than 0.15 mol m^{-3}, the reaction rate was controlled by the flux of oxygen to the TiO_2 surface. For oxygen concentrations in the range of 0.15–0.94 mol m^{-3}, the rate was controlled simultaneously by the flux of both oxygen and photons.

The concentration profile of oxygen in the diffusion layer along the reactor plate was calculated assuming that oxygen molecule reacts with electrons on the TiO_2 surface. A reaction order 0.25 was confirmed which indicates that the reaction of oxygen with electrons is a heterogenous reaction decelerated by internal diffusion in the porous structure of the immobilised photocatalyst film. The results confirm the assumed effect of oxygen transfer to the semiconductor surface on the overall rate of photocatalysis.

Acknowledgement

The authors thank the Grant Agency of the Czech Republic for financial support (grant 203/96/088 and 203/99/0763).

References

1. K.W. Boer, 'Survey of Semiconductor Physics' (Van Nostrand–Reinhold, New York, 1990), p. 249.
2. M. Grätzel, 'Heterogeneous Photochemical Electron Transfer' (CRC Press, Boca Raton, FL, 1989).
3. M.V. Rao, K. Rajeshwar, V.R. Vernerker and J. Dubow, *J. Phys. Chem.* **84** (1980) 1987.
4. S. Nishimoto, B. Ohtani, H. Kajiwara and T. Kagiya, *J. Chem. Soc., Faraday Trans. 1* **81** (1985) 61.
5. G. Mills and M.R. Hoffmann, *Environ. Sci. Technol.* **27** (1993) 1681.
6. C. Kormann, D.W. Bahnemann and M.R. Hoffmann, *Environ. Sci. Technol.* **25** (1991) 494.
7. E.R. Carraway, A.J. Hoffmann and M. R. Hoffmann, *Environ. Sci. Technol.* **28** (1994) 786.
8. A. Chemeseddine and H.P. Boehm, *J. Mol. Catal.* **60** (1990) 295.
9. J.C. D'Oliveira, C. Minero, E. Pelizzetti and P. Pichat, *J. Photochem. Photobiol. A: Chem.* **72** (1993) 261.
10. H. Hidaka, J. Zhao, E. Pelizzetti and N. Serpone, *J. Phys. Chem.* **96** (1992) 2226.
11. E. Pelizzetti, C. Minero, P. Piccinini and M. Vincenti, *Coord. Chem. Rev.* **125** (1993) 183.
12. M.R. Hoffmann, S.T. Martin, W. Choi and D.W. Bahnemann, *Chem. Rev.* **95** (1995) 69.
13. C.S. Turchi and M.S. Mehos, *in* 'Chemical Oxidation: Technology for the Nineties', Second International Symposium, Nashville, TN (1992).
14. S.L. Wilkinson and W.A. Anderson, Abstracts of the First International Conference on 'Advanced Oxidation Technologies for Water and Air Oxidation', London, Ontario, Canada, 25–30 June (1994), p. 299.
15. K. Hashimoto and A. Fujishima, Abstracts, *op. cit.* [14], p. 311.
16. J.F. Kenneke and W.H. Glatze, Proceedings of the Symposium on 'Water Purification by Photocatalytic, Photoelectrochemical and Electrochemical Process', The Electrochemical Society **94** (1994) 365.
17. D. Bockelmann, 'Photocatalytical Solar Treatment of Waste Water', PhD thesis, (Technical University Clausthal, Germany, 1993).
18. I.M. Butterfield, P.A. Christensen A. Hamnett, K.E. Shaw, G.M. Walker and S.A. Walker, *J. Appl. Electrochem.* **27** (1997) 385.
19. P.A. Christensen and G.M. Walker, 'Opportunities for the UK in Solar Detoxification', ETSU S/P4/00249/REP (ETSU 1996).
20. H. Gerischer and A. Heller, *J. Electrochem. Soc.* **139** (1992) 113.
21. J. Kulas, I. Roušar, J. Krýsa and J. Jirkovský, *J. Appl. Electrochem.* **28** (1998) 843.
22. J. Krýsa, L. Vodehnal and J. Jirkovský, *J. Appl. Electrochem*, **29** (1999) 429.
23. J.F. Rabek, 'Experimental Methods in Photochemistry and Photophysics', Part II. (J. Wiley & Sons, New York, 1982, p. 945).
24. K. Bouzek and I. Roušar, *J. Chem. Technol. Biotechnol.* **66** (1996) 131.